Smart Mater. Struct. 7 (1998) 720–731. Printed in the UK PII: S0964-1726(98)96185-7

Comparative study of damage identification algorithms applied to a bridge: II. Numerical study*

Charles R Farrar† and David A Jauregui‡

† Engineering Analysis Group, Los Alamos National Laboratory, Los Alamos, NM, USA
‡ Department of Civil Engineering, University of Texas, Austin, TX, USA

Received 14 March 1997, accepted for publication 14 July 1997

Abstract. This paper extends the study of damage identification algorithms summarized in the accompanying paper 'Comparative study of damage identification algorithms: I. Experiment' to numerical examples. A finite element model of a continuous three-span portion of the I-40 bridges, which once crossed the Rio Grande in Albuquerque, NM, was constructed. Dynamic properties (resonant frequencies and mode shapes) of the undamaged and damaged bridge that were predicted by the numerical models were then correlated with experimental modal analysis results. Once correlated with the experimental results, eight new damage scenarios were introduced into the numerical model including a multiple damage case. Also, results from two undamaged cases were used to study the possibility that the damage identification methods would produce false-positive readings. In all cases analytical modal parameters were extracted from time-history analyses using signal processing techniques similar to those used in the experimental investigation. This study provides further comparisons of the relative accuracy of these different damage identification methods when they are applied to a set of standard numerical problems.

1. Introduction

An accompanying paper (Farrar and Jauregui 1998) describes a study where five different damage identification algorithms were applied to modal data obtained from an undamaged and subsequently damaged, full scale interstate highway bridge (the I-40 bridge over the Rio Grande in Albuquerque, NM). The direct comparison of different damage detection algorithms, when applied to the same data, provides insight into the relative merits of these various algorithms. However, the costs, time constraints associated with this type of testing and the inability to repair the damage after it was introduced limited these tests such that only one damage location was investigated.

To extend the comparative study of global, modal-based damage detection methods, a finite element model of the I-40 bridge was developed and correlated with modal data obtained from vibration tests performed on the undamaged structure (Farrar *et al* 1994). Additional linear damage scenarios were introduced into this model at various locations. Simulated modal tests were then performed numerically. The term linear used to describe the damage scenarios because a linear finite element model was used to model the structure both before and after damage. Damage introduced into the actual structure was also considered linear because the torch cuts described in the accompanying paper produced simulated cracks too wide to open and close when the bridge was subjected to dynamic loading during the experimental modal analyses. Data from the numerically simulated tests were then analysed using the same five damage detection methods that had previously been applied to the experimental data. This paper summarizes the results of the numerical damage detection studies performed with the finite element model of the I-40 bridge. In all subsequent discussions, rather than reference the accompanying paper every time this study is compared to the experimental work, the reader is assumed to be cognizant that the experimental work is described in the accompanying paper and in more detail in Farrar *et al* (1994) and Farrar and Jauregui (1996). The reader is again referred to the accompanying paper for a detailed description of the I-40 bridge geometry and a summary of other previous damage detection studies performed on bridges. A thorough review of global damage detection based on changes in modal properties, including limitations and successes of these methods, can be found in Doebling *et al* (1996).

* Work performed under the auspices of the US Department of Energy.

0964-1726/98/050720+12$19.50

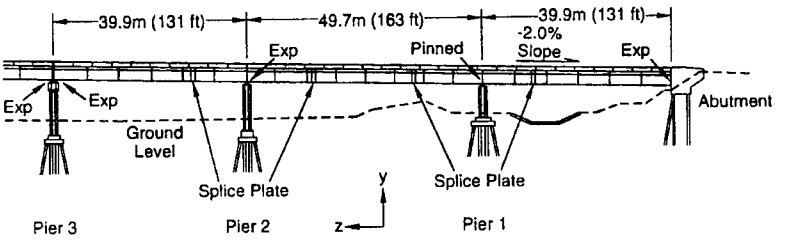

Figure 1. Elevation view of the portion of the I-40 bridge that was tested.

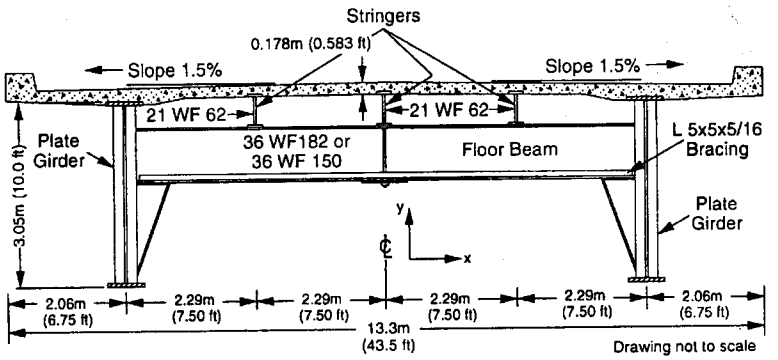

Figure 2. Cross-section geometry of the I-40 bridge.

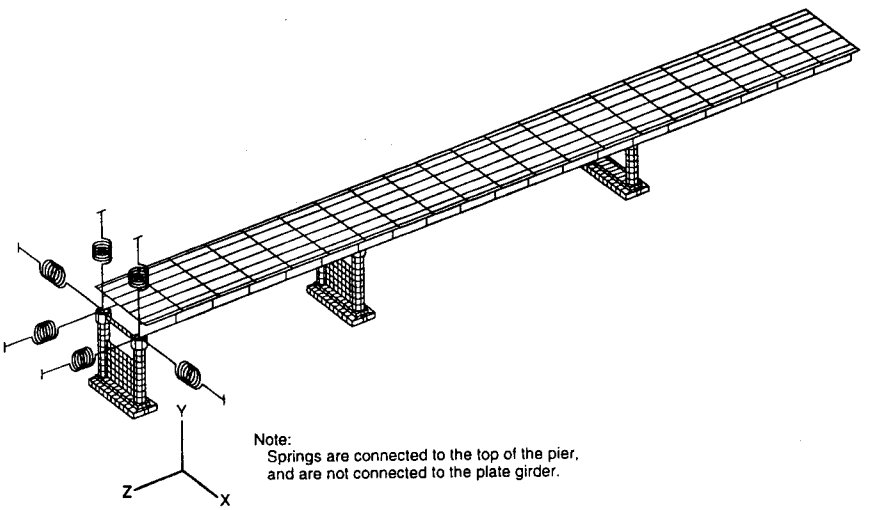

Figure 3. Finite element model of the portion of the I-40 bridge on which experimental modal analyses were performed.

2. Numerical model of the I-40 bridge

Using correlated finite element models, forced vibration tests similar to the ones conducted on the I-40 bridge were simulated numerically. All dynamic analysis calculations were performed with the ABAQUS standard finite element code (Hibbitt, Karlsson and Sorensen 1994) on a CRAY Y-MP computer. Results from these analyses (node point accelerations) were then analysed using similar signal processing techniques to those applied to the experimental accelerometer data. Signal processing tasks were performed using MATLAB Standard (MathWorks 1992a, b) and the MATLAB Signal Processing Toolbox (MathWorks 1992c).

2.1. Finite element discretization

The portion of the I-40 bridge that was studied is shown in figure 1 and the cross-section geometry is shown in figure 2. Figure 3 shows the finite element model of this portion of the I-40 bridge. Spring elements were added to the end pier to simulate the stiffness contributions of the next section of the bridge that shared this common pier. Eight-node shell elements were used to model the web of the two plate girders and the concrete deck. Three-node beam elements were used to model the girder flanges, the floor beams and the stringers. Horizontal and vertical stiffeners on the plate girder, the diagonal bracing and the concrete reinforcement were not included in this model. Previous

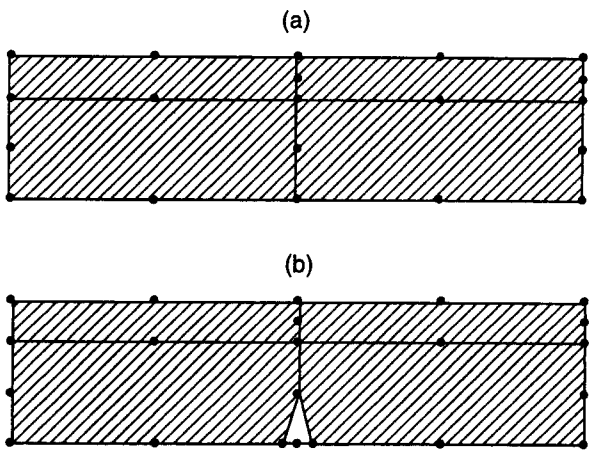

Figure 4. Finite element modeling of the north plate girder (a) before damage and (b) after damage.

studies (Farrar *et al* 1996) where the individual stiffeners were modeled showed no significant variation in the global dynamic properties from the model used in this study. The finite element model simulates composite action between the concrete deck, the stringers and the plate girders.

Generic material properties for steel were specified as $E_{steel} = 200$ GPa (29 000 000 psi), $\nu_{steel} = 0.3$ and $\mu_{steel} = 38.2$ g cm^{-3} (0.284 lbm in^{-3}). Generic concrete properties were specified as $E_{concrete} = 24.8$ GPa (3 600 000 psi), $\nu_{concrete} = 0.2$ and $\mu_{concrete} = 2320$ kg m^{-3} (145 lbm ft^{-3}).

2.2. Simulation of experimental damage scenarios

As shown in figure 4, three levels of damage similar to the final three girder cuts imposed during the I-40 bridge tests were simulated by creating additional nodes at the vicinity of the crack and redefining the finite element discretization of the plate girder web and bottom flange in this region.

The second level of damage (corresponding to experimental damage case E-2) was simulated by disconnecting the shell elements representing the lower one-third of the web and allowing the bottom flange to remain connected using a new beam element. For the third phase of damage (corresponding to experimental damage case E-3), the new beam element directly below the termination of the web cut is altered to one-half its original cross-sectional area. Finally, the new bottom flange element connecting the two damaged portions of the girder was removed to simulate the final damage condition (corresponding to experimental damage case E-4). This method of modeling the damage changes the geometry only, and does not introduce nonlinearities into the model. Therefore, a linear modal analysis can be performed to ascertain the effects of this damage on the dynamic properties of the structure.

2.3. Correlation with measured modal properties

To correlate the dynamic response predicted by the finite element model to dynamic response measured on the bridge, the calculated resonant frequencies and mode shapes for both the damaged and undamaged bridge models were compared to the corresponding quantities measured on the bridge. Undamped modal analyses were performed on the finite element model to determine the resonant frequencies and mode shapes. Correlation was obtained by adjusting the stiffness of the springs used to model the structural effects contributed by the next section of the bridge that shares the common pier; by adjusting the boundary conditions applied to the base of the plate girder where it would rest on the abutment and by adjusting the restraints between the bottom flange of the plate girder and the top of the concrete piers.

The model that best agreed with the measured results in terms of both the measured resonant frequencies and the measured mode shapes had the following attributes. At the abutment, nodes at the bottom plate girder flanges were constrained against translation in the X and Y directions (shown in figure 1). Rotations about the Y and Z axes were also constrained at these locations. The nodes corresponding to the bottom of the plate girder at piers 1, 2 and 3 were constrained to have the same translation in the X, Y and Z directions as the nodes representing the top and center of the respective pier column. At all the piers, no constraints were imposed on the rotational degrees of freedom. Springs used to simulate the stiffening effects of the other portion of the bridge sharing pier 3 were not used.

The comparison of resonant frequencies calculated with this model and those measured on the structure for both the undamaged and damaged cases is summarized in table 1. A modal assurance criterion (MAC) (Ewins 1985) is used to compare the mode shapes and these results are summarized in table 2. The MAC makes use of the orthogonality properties of the mode shapes to compare two modes. If the modes are identical, a scalar value of one is calculated by the MAC. If the modes are orthogonal and dissimilar, a value of zero is calculated. The MAC that compares mode i and j has the form

$$\mathrm{MAC}(i,\ j) = \frac{|\sum_{k=1}^{n}(\phi_j)_k(\phi_i)_k^*|^2}{(\sum_{k=1}^{n}(\phi_j)_k(\phi_j)_k^*)(\sum_{k=1}^{n}(\phi_i)_k(\phi_i)_k^*)} \quad (1)$$

where $(\phi)_k$ is an element of the mode-shape vector and the asterisk denotes complex conjugate. Ewins points out that, in practice, correlated modes will yield a value greater than 0.9, and uncorrelated modes will yield a value less than 0.05. To make this comparison, the components of the analytical mode shape vectors corresponding to translation in the vertical direction at locations similar to the accelerometer locations were extracted from the finite element analysis to form a mode-shape vector that could be directly compared to the experimentally measured mode shapes.

Table 1 shows that the resonant frequencies do not change appreciably until the final stage of damage has been introduced. This result is shown in both the experimental data and the numerical calculations. No change in the mode shapes can be seen until the final stage of damage as is indicated by both the analytical and experimental mode-shape data summarized in table 2. It is of interest to note that after the final stage of damage, modes 1 and 2 determined by finite element analysis showed almost the same percent drop in resonant frequency from their undamaged state as the corresponding drops in resonant frequencies measured on the bridge.

Table 1. Resonant frequencies measured on the damaged bridge compared with resonant frequencies calculated by finite element analyses of the damaged structures.

	Undamaged structure		2nd level of damage (E-2)[a], 6 ft cut in web		3rd level of damage (E-3)[a], 6 ft cut in web, cut through half of the bottom flange		Final level of damage (E-4)[a], 6 ft cut in web, cut through entire bottom flange	
Mode	Measured (test t16tr)[a]	F.E. results	Measured (test t18tr)[a]	F.E. results	Measured (test t19tr)[a]	F.E. results	Measured (test t22tr)[a]	F.E. results
1	2.48	2.59	2.52	2.59	2.46	2.59	2.30	2.44
2	2.96	2.78	2.99	2.78	2.95	2.78	2.84	2.72
3	3.50	3.71	3.52	3.71	3.48	3.71	3.49	3.71
4	4.08	4.32	4.09	4.33	4.04	4.33	3.99	4.27
5	4.17	3.96	4.19	3.96	4.14	3.96	4.15	3.96
6	4.63	4.50	4.66	4.50	4.58	4.50	4.52	4.46
Ave. % diff.		5.04%		5.00%		5.15%		4.92%

[a] Damage case designations and test designations correspond to those described in the accompanying paper.

Table 2. Modal assurance criterion comparing the measured mode shapes from the damaged bridge with mode shapes calculated by finite element analysis.

Mode	1	2	3	4	5	6
test t16tr[a] × undamaged finite element model						
1	0.992	0.001	0.000	0.001	0.003	0.000
2	0.003	0.983	0.000	0.010	0.002	0.008
3	0.001	0.000	0.993	0.001	0.002	0.000
4	0.010	0.000	0.001	0.035	0.960	0.000
5	0.000	0.000	0.010	0.978	0.005	0.029
6	0.001	0.010	0.000	0.001	0.018	0.954
test t18tr[a] × finite element model simulating second damage level						
1	0.988	0.002	0.000	0.001	0.004	0.000
2	0.001	0.989	0.000	0.005	0.001	0.011
3	0.000	0.000	0.994	0.001	0.002	0.000
4	0.011	0.001	0.000	0.015	0.980	0.002
5	0.000	0.000	0.014	0.977	0.005	0.019
6	0.001	0.012	0.000	0.001	0.012	0.950
test t19tr[a] × finite element model simulating third damage level						
1	0.994	0.000	0.000	0.001	0.005	0.000
2	0.001	0.988	0.000	0.004	0.001	0.011
3	0.000	0.000	0.994	0.001	0.002	0.001
4	0.011	0.001	0.000	0.012	0.983	0.002
5	0.000	0.000	0.010	0.982	0.005	0.017
6	0.001	0.006	0.000	0.002	0.011	0.962
test t22tr[a] × finite element model simulating final damage level						
1	0.981	0.005	0.001	0.000	0.001	0.002
2	0.025	0.973	0.000	0.002	0.007	0.007
3	0.000	0.000	0.996	0.000	0.001	0.001
4	0.016	0.000	0.001	0.007	0.947	0.074
5	0.000	0.000	0.008	0.986	0.007	0.011
6	0.002	0.004	0.001	0.001	0.049	0.878

[a] Test designations correspond to those described in the accompanying paper.

The calculated mode shapes were found to be particularly sensitive to the boundary conditioned used to model the connection of the plate girder to the abutment. With the boundary conditions described above specified, the finite element model calculated the mode corresponding to the measured mode 5 at a lower frequency than the mode corresponding to the measured mode 4. When the springs that model the stiffening effects of the next section of bridge were added, the average resonant frequency error dropped to less than two percent and modes 4 and 5 were in the order corresponding to the measured results. However, these mode shapes, in general, did not agree as well with the measured data. Hence, boundary conditions that provide the most accurate model in terms of correlation between measured and calculated resonant frequencies were not the same boundary conditions that provided the best correspondence between the calculated and measured mode shapes. The discrepancies with experimental results shown in tables 1 and 2, which are considered small, are assumed to be primarily caused by the idealization of the boundary conditions and the use of generic material properties for the concrete portion of the bridge. The authors feel that, for the purpose of a comparative study of damage detection algorithms, adequate agreement with measured dynamic properties was obtained. Hence, systematic model-updating techniques were not employed.

2.4. Simplifications

After the finite element model was shown to predict dynamic properties similar to those measured on the I-40 bridge, both in its damaged and undamaged condition, the piers were removed from the model in the interest of reducing computational time. Because this study is interested in the relative performance of different damage detection methods, it was assumed that removing the piers would not adversely affect the intended purpose of this study. The resulting finite element model of the bridge superstructure, figure 5, had 7032 degrees of freedom.

Boundary conditions were enforced at the support locations shown in figure 5 where the bridge was previously supported by the concrete piers. At all support locations, translations in the three global directions X, Y and Z were constrained. To further simulate the actual support conditions at the base of the plate girders above the piers,

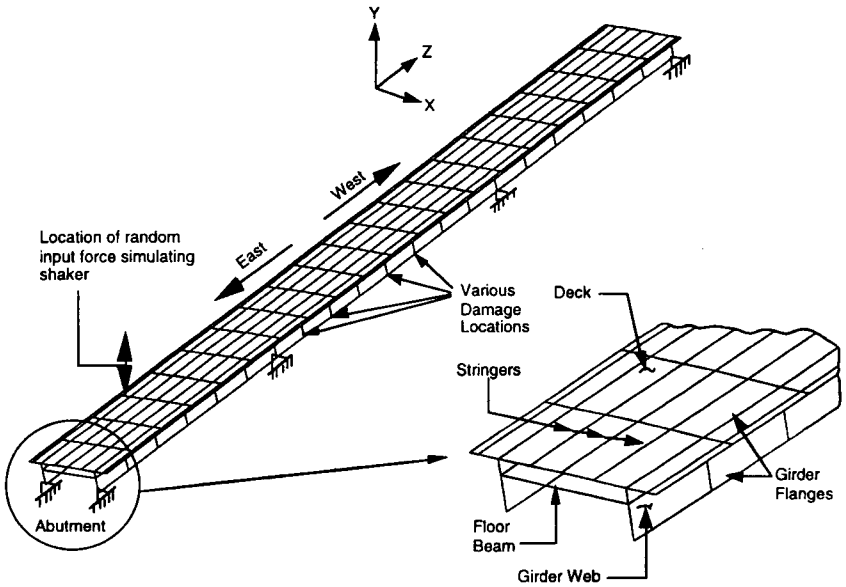

Figure 5. Finite element model of the three-span unit of the I-40 bridge, neglecting the piers.

the out-of-plane rotations (about the Y and Z axes shown in figure 5) are also constrained at these locations.

2.5. Additional damage cases

As a supplement to the damage simulations at the girder mid-span, other damage scenarios were modeled to evaluate the dynamic response of the bridge with damage at different locations. Five additional damage scenarios were modeled at different locations on the north girder in the center span. These additional conditions are:

(1) One plate girder cut simulating the final experimental damage case positioned halfway between mid-span and the east interior support.

(2) One plate girder cut simulating the final experimental damage case positioned one floor-beam-panel away from the east interior support.

(3) Two plate girder cuts, each simulating the final experimental damage case, positioned two floor-beam-panels away from the east interior support and three floor-beam-panels away from the west interior support.

(4) One plate girder cut simulating the second experimental damage case positioned halfway between mid-span and the east interior support.

(5) One plate girder cut simulating the second experimental damage case positioned one floor-beam-panel away from the east interior support.

A summary of the numerically simulated damage cases is provided in table 3.

2.6. Time-history analyses

For the I-40 bridge vibration tests, a 8.90 kN (2000 lb) peak-amplitude random excitation was applied to the structure. A random signal was generated to simulate the input force applied by the shaker during the actual experimental modal testing of the I-40 bridge. The signal

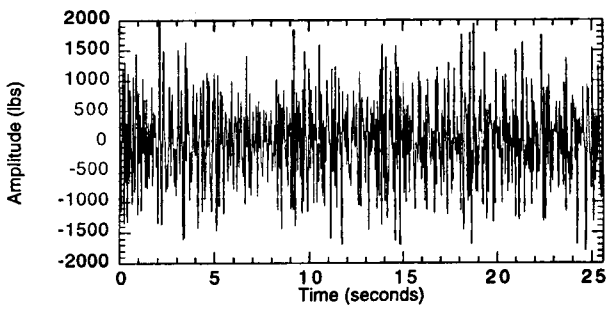

Figure 6. Generated random signal representing the input force applied by the shaker.

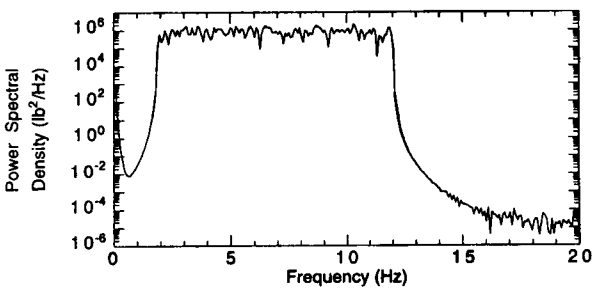

Figure 7. Power spectral density of the random input force in the frequency range of 0 to 20 Hz.

was specified so that it would have a uniform power spectral density (PSD) in the range of 2 to 12 Hz and a peak amplitude of 8.90 kN (2000 lb). The random signal was defined by 1024 data points at 0.025 s increments. Plots of the generated random signal along with its PSD are provided in figures 6 and 7, respectively. The random force was applied as a time-varying concentrated vertical load on the concrete deck directly above the south girder at the midpoint of the east span as shown in figure 5.

The time-history response of the structure subjected to this random excitation was calculated using modal

Table 3. Summary of numerically simulated damage cases.

Damage case designation	Location of damage	Damage description
A-1	mid-span	lower one-third portion of web cut
A-2	mid-span	lower one-third portion of web plus half of bottom flange cut
A-3	mid-span	lower one-third portion of web plus entire bottom flange cut
A-4	one location: halfway between mid-span and east support	lower one-third portion of web plus entire bottom flange cut
A-5	one location: one floor-beam-panel away from east support	lower one-third portion of web plus entire bottom flange cut
A-6	two locations: halfway between mid-spans and east support; one floor-beam-panel west of mid-span	lower one-third portion of web plus entire bottom flange cut
A-7	one location: halfway between mid-span and east support	lower one-third portion of web cut
A-8	one location: one floor-beam-panel away from east support	lower one-third portion of web cut

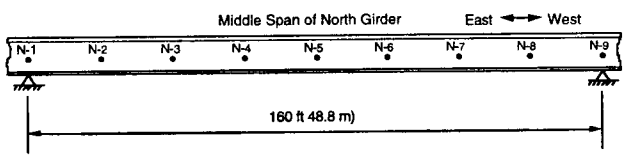

Figure 8. Enlarged view of the central span of the I-40 bridge showing the simulated accelerometer locations N-1 through N-9.

superposition. The first ten modes were used to perform this calculation. Approximately 1.5 h of cpu time on a CRAY Y-MP computer were required to calculate 1024 time-history response points. Nine equally spaced nodal points were monitored to simulate the experimental accelerometer locations. Figure 8 shows an enlarged view of the bridge central span highlighting these locations. The numerical accelerometer locations are spaced longitudinally at equal distances of approximately 6.1 m (20 ft), which are locations where the floor beams frame into the main girder. In the vertical direction, the monitored nodes are located approximately one-third of the girder height above the bottom flange. The forced-vibration dynamic analysis was initially done with the bridge in its undamaged state and then repeated for each damaged case A-1 through A-8.

2.7. Simulated experimental modal analysis

With node point acceleration–time histories determined by forced vibration dynamic analyses, a simulated experimental modal analysis was conducted using the nine measured responses shown in figure 8. For this analysis node N-3 was designated as the reference location. The 1024-point time histories from the nine response locations were divided into two 512-point signals. A Hanning window was applied to each 512-point signal and the signal was transformed into the frequency domain with a fast Fourier transform algorithm. The resulting frequency-domain signals were then averaged and used to compute individual PSDs and the cross-power spectral densities (CPSDs) between the various signals and the reference signal. Processing the calculated response time histories in this manner simulates the signal processing approach that would be employed to compute modal properties from ambient vibration data.

The sampling parameters used in this study consisted of 25.6 s time windows discretized with 1024 samples. With these sampling parameters a frequency resolution 0f 0.0781 Hz was obtained for the CPSD over a frequency range of 0–20 Hz. Resonant frequencies were determined from frequencies corresponding to peaks in the CPSD. Complex mode shapes were determined from the magnitude and phase of the CPSDs between the nine channels, N-1 through N-9, relative to the reference response N-3 (see figure 8). The amplitude of a mode shape was determined from the magnitude of the CPSD at the mode's associated resonant frequency. Because no damping was specified in these analyses, phase angles of the CPSDs at resonance were either 0 or 180 degrees and the phase information

was incorporated into the mode shape data by specifying each amplitude as either a positive (0 degrees) or negative value (180 degrees).

The mode shape data were then normalized assuming an identity mass matrix as discussed in Clough and Penzien (1993), hence the modal vectors were required to satisfy the condition

$$\{\phi_n\}^T[m]\{\phi_n\} = 1 \tag{2}$$

where $\{\phi_n\}$ is the normalized modal vector and $[m]$ the mass matrix = diag(1).

Letting ψ_n represent the original modal amplitudes obtained from the simulated ambient modal analysis, the normalized magnitudes are computed using the equation

$$\{\phi_n\} = \frac{1}{\sqrt{M_n}}\{\psi_n\} \tag{3}$$

where

$$M_n = \sum_{i=1}^{p} \psi_{in}^2 m_i. \tag{4}$$

In the latter equation, p is the number of measured points, n the mode shape number.

2.8. False-positive studies

The final case (A-9) did not involve altering the finite element model. Instead, the original forcing function is replaced with a different random time history that had the same peak amplitude and the same frequency content. Note that although the force time histories differ between the alternate and original random force, their frequency contents remain similar. This case was included in the investigation to test that the damage identification routines do not identify damage when two different undamaged responses are analysed, that is, give a 'false-positive' reading.

3. Influence of damage on conventional modal properties

Before conducting the forced vibration dynamic analyses of the I-40 bridge, eigenvalue analyses were performed to identify the resonant frequencies of the first three modes of the bridge. An analysis was first conducted with the bridge in an undamaged condition and then repeated for each state of damage (cases A-1 through A-8) to determine the changes, if any, in the resonant frequencies that resulted from the damage.

In general, changes in the mode shapes and resonant frequencies could only be observed for the most severe level of damage (cases A-3–A-6). As an example, figure 9 shows the first bending mode identified from the eigenvalue analysis of the undamaged bridge. The same mode identified for damage case A-3 is shown in figure 10. When this level of damage is introduced, there is a decrease in the resonant frequency of the first mode (approximately 4.2%) along with a 0.78% reduction for the second mode frequency. No changes were detected in the third mode frequency after damage case A-3 was introduced. This result was expected because one of the nodes for the third mode coincided with the damage location. Table 4 summarizes the changes in resonant frequencies for the first three modes that resulted from the various damage scenarios.

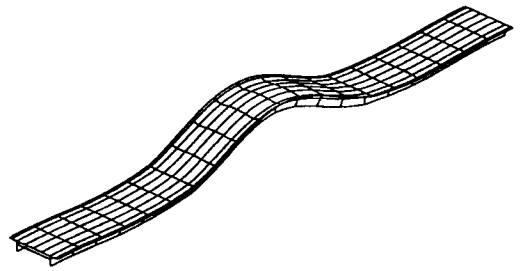

Figure 9. First bending mode identified from eigenvalue analysis of the undamaged bridge.

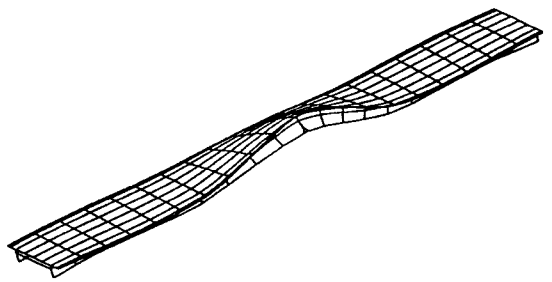

Figure 10. First bending mode identified from eigenvalue analysis of the damaged bridge, case A-3.

4. Application of damage detection algorithms to numerical data

The same five damage identification algorithms that were applied to the experimental data in the accompanying paper were also applied to the numerically generated data. These damage detection methods and their implementation are described in the accompanying paper. A more detailed summary of these methods can be found in the papers referenced below and in Farrar and Jauregui (1996). The five methods that were compared are the damage index method (Stubbs and Kim 1994); the change in mode shape curvature method (Pandey *et al* 1991); the change in flexibility method (Pandey and Biswas 1994); the change in uniform load surface curvature method (Zhang and Aktan 1995) and the change in stiffness method (Zimmerman and Kaouk 1994).

Figures 11 through 15 show the results of applying the various damage identification methods to damage case A-6 where two damage locations were specified in the numerical model. While the specific magnitudes of the various damage indices cannot be directly compared, for all methods damage is indicated by the peak change in the respective monitored modal-based parameter. The damage in this case corresponded to a cut completely through the bottom flange. The actual damage locations for case A-6 are nodes 40 and 100. All the methods give indications of damage at these locations. However, the damage

Table 4. Resonant frequencies calculated by finite element analyses of the various damage scenarios.

Damage case	First bending mode Freq. (Hz)[a]	First torsional mode Freq. (Hz)[a]	Second bending mode Freq. (Hz)[a]
Undamaged	3.79	3.87	5.09
A-1	3.79 (0.0%)	3.87 (0.0%)	5.09 (0.0%)
A-2	3.79 (0.0%)	3.87 (0.0%)	5.09 (0.0%)
A-3	3.63 (4.2%)	3.84 (0.78%)	5.09 (0.0%)
A-4	3.79 (0.0%)	3.87 (0.0%)	5.07 (0.4%)
A-5	3.63 (4.2%)	3.85 (0.5%)	5.07 (0.4%)
A-6	3.69 (2.6%)	3.85 (0.5%)	5.07 (0.4%)
A-7	3.79 (0.0%)	3.87 (0.0%)	5.09 (0.0%)
A-8	3.79 (0.0%)	3.87 (0.0%)	5.09 (0.0%)

[a] Values in parentheses are the percent change from the undamaged case.

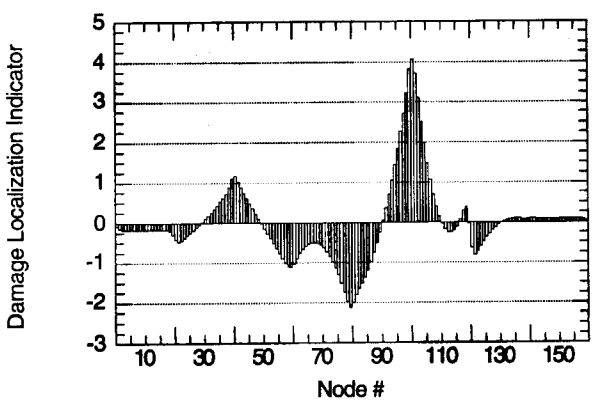

Figure 11. Damage index method applied to case A-6.

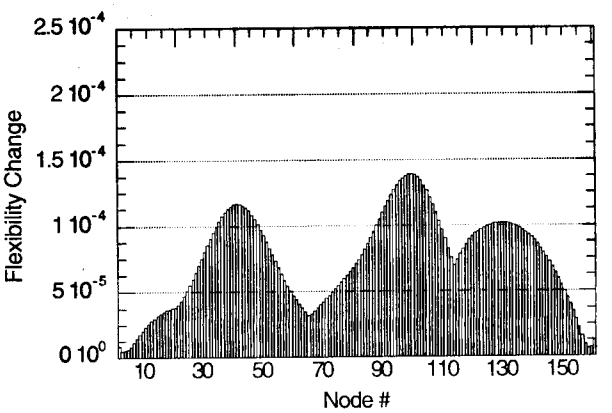

Figure 13. Change in flexibility method applied to case A-6.

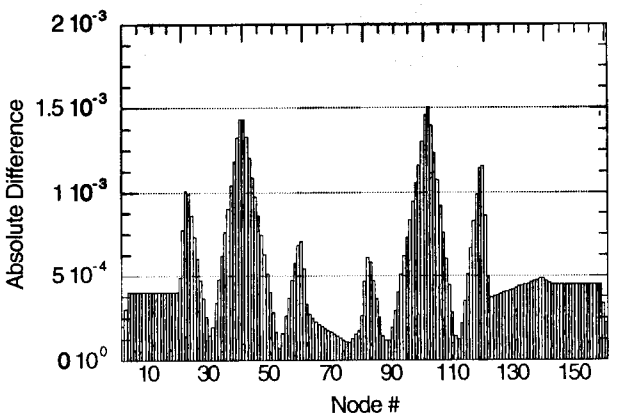

Figure 12. Change in mode curvature method applied to case A-6.

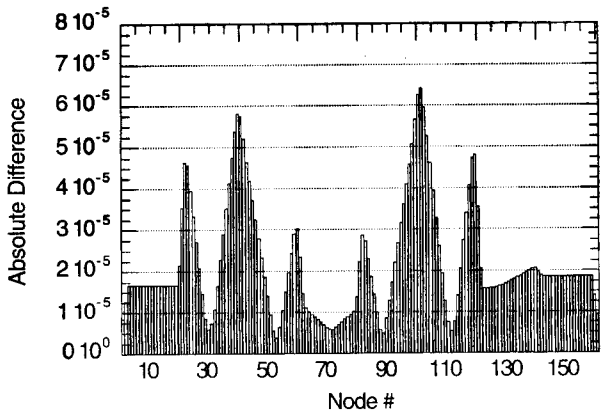

Figure 14. Change in uniform load surface curvature method applied to case A-6.

index method does not yield a value greater than 2 (the probability-based criterion for damage) at node 40.

Figure 16 shows the results of the damage index method applied to damage case A-1 which simulated a cut through the bottom one-third of the plate girder web at mid-span. From figure 16 it is clear that the damage index method has located the damage, but this method has also indicated another damage location at node 20. This result was not anticipated because this method successfully and

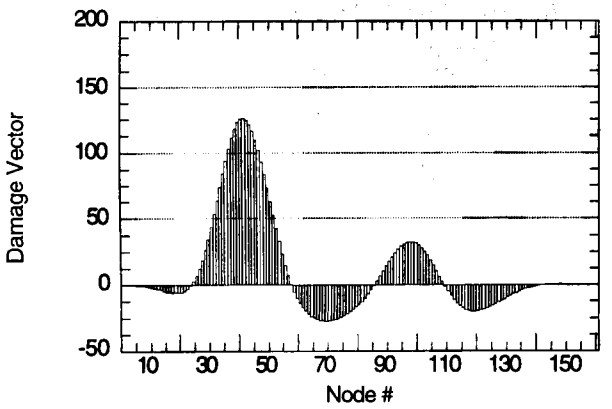

Figure 15. Change in stiffness method applied to case A-6.

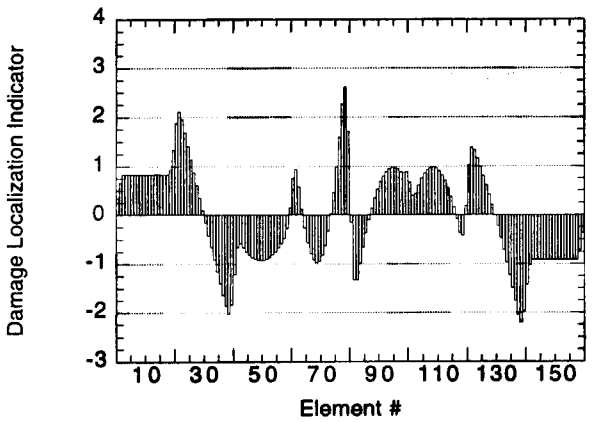

Figure 16. Damage index method applied to case A-1.

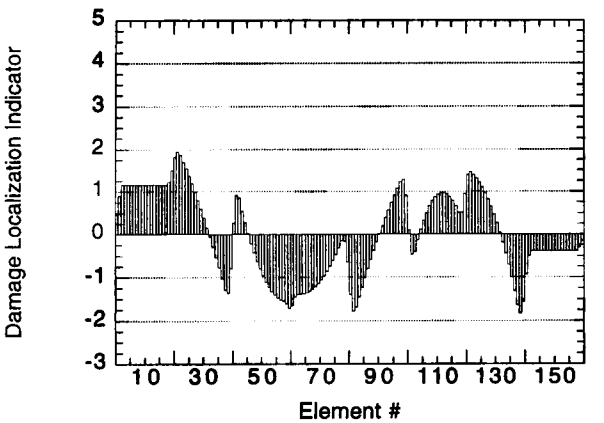

Figure 17. Damage index method applied to the two undamaged data sets, case A-9.

unambiguously located the less severe experimental damage case 1. This discrepancy suggests the need for statistical analysis procedures to determine if changes in measured modal quantities are statistically meaningful. Statistical methods will aid in determining whether the changes in modal properties can be attributed to damage or whether they are within the repeatability of the test.

Figures 17 through 21 show the results of applying the various damage detection methods to the two undamaged data sets, damage case A-9. Using the criterion that the

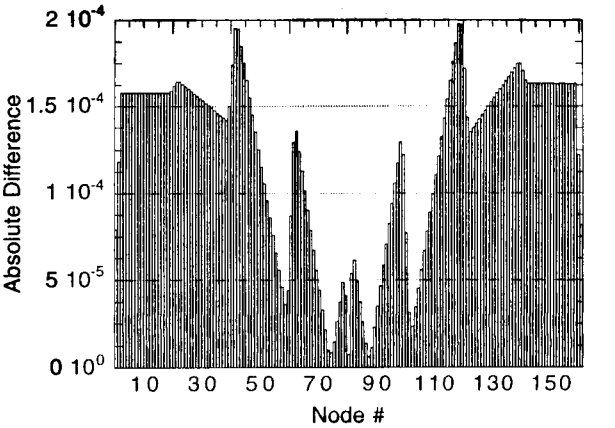

Figure 18. The change in mode shape curvature method applied to the two undamaged data sets, case A-9.

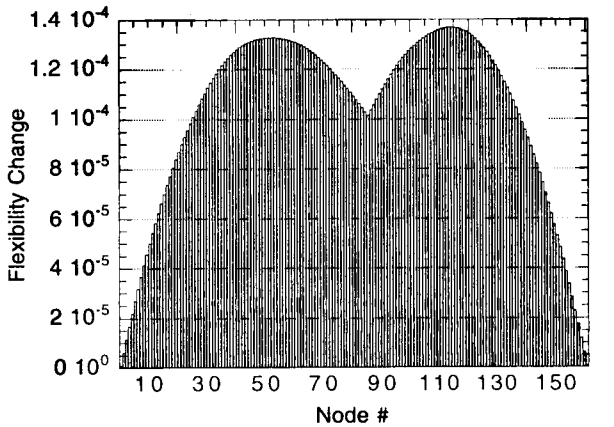

Figure 19. The change in flexibility method applied to the two undamaged data sets, case A-9.

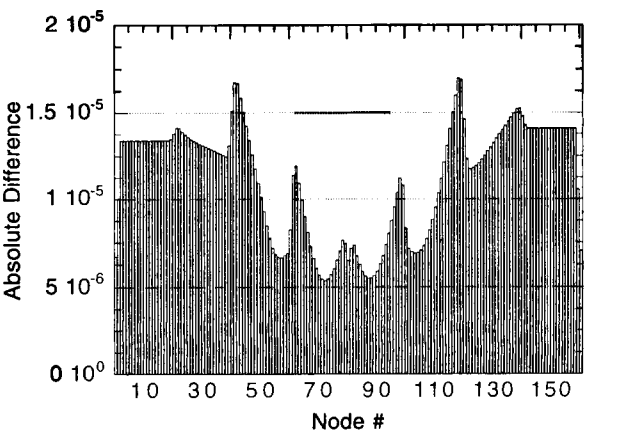

Figure 20. The change in uniform load surface curvature method applied to the two undamaged data sets, case A-9.

damage indicator must be greater than two to be indicative of damage, the damage index method does not give a false-positive indication of damage as shown in figure 17. A value of two is almost reached at location 20, which corresponds to a location where the flange dimensions of the plate girders abruptly change. However, similar values are not recorded at the other location where the flange dimensions change abruptly (location 140). The other four

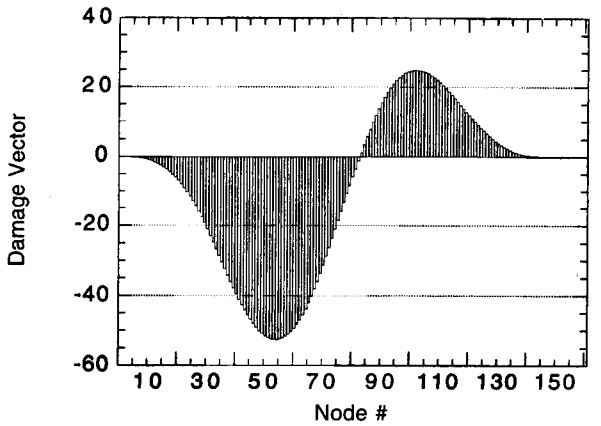

Figure 21. The change in stiffness method applied to the two undamaged data sets, case A-9.

damage detection methods yield ambiguous results when they are applied to the two different undamaged data sets. If applied blindly, the results shown in figures 18 through 21 could be interpreted to give false-positive indications of damage.

A complete set of plots corresponding to each damage detection method applied to each damage case can be found in Farrar and Jauregui (1996). Table 5 summarizes the results obtained when the various damage identification methods were applied to the data sets corresponding to each damage case and the case where two undamaged data sets were analysed.

5. Summary and conclusions

A study was undertaken to extend the comparison of five damage identification methods that were previously applied to experimental data measured on the I-40 bridge over the Rio Grande in Albuquerque, NM. After benchmarking a finite element model against measured modal data from a bridge in its undamaged and damaged conditions, extensive numerical studies were performed to further evaluate the various damage detection techniques that had previously been applied to the experimental data. Nodal point accelerations, at locations corresponding to the experimental accelerometer locations, were calculated from the finite element analyses, and then processed to yield mode shape and resonant frequency data. It is the authors' opinion that if automated damage identification methods are to become an accepted part of a comprehensive bridge management system, these methods will have to monitor the response of a bridge to ambient (typically traffic-induced) vibration. To this end, the data reduction methods used in this study have assumed that the input is not monitored.

Five damage identification algorithms were applied to the numerically generated modal data from finite element simulations of the undamaged and damaged bridge. All the algorithms require undamaged and damaged mode shape data. In addition, some of the methods require undamaged and damaged resonant frequencies as well as unit-mass-normalized mode shapes. Although not rigorously verified, it appeared that using an assumed identity mass matrix to normalize the modes did not adversely affect these methods. This result is attributed to the fact that the measured modes resemble beam-like response and that the mass of the bridge is uniformly distributed along the longitudinal axis of this 'beam'. However, results from the accompanying experimental study indicated that some methods performed better when they were applied to unit-mass-normalized mode shape data.

In general, all methods identified the various damage locations correctly for a cut completely through the bottom flange (A-3 through A-6). However, for several of these methods, if they had been applied blindly, it would be difficult to tell whether damage had not occurred at locations other than the actual one. The methods were inconsistent and did not clearly identify the damage location when they were applied to the less severe damage cases (A-1, A-2, A-7, A-8). Results of this study show that the damage index method performed the best when the entire set of analyses is considered. This performance is attributed to the methods of normalizing changes in the parameters that are used to indicate damage, that is, curvature of the mode shape, relative to the undamaged values.

In choosing the damage identification methods to be compared, the authors have limited their study to those requiring only measured responses before and after damage as opposed to those requiring a correlated finite element model. Although the finite element models in this study were benchmarked against measured modal data, this benchmarking was done only to verify that the models were accurately predicting the dynamic response of the structure. Model-updating damage identification methods, which require correlated finite element models, were not used in this study because it is the authors' opinion that it would be impractical to develop correlated finite element models for a large population of bridges.

Except for the damage index method, all the methods studied gave false-positive indications of damage when they were applied to the two undamaged data sets. Although not analytically verified, it is assumed that the false-positive readings could be eliminated by taking more averages of the data used to obtain the cross-power spectral density function and, in turn, the mode shape amplitudes. The probabilistic-based criterion employed by the damage index method for determining whether change in the monitored parameter is indicative of damage is attributed with eliminating the false-positive reading when this method was applied to these data sets. For the other methods, the comparison of two undamaged data sets can be used to establish the minimum levels of change in the monitored parameter that damage must produce before it can be detected.

Another observation from this study, which the authors feel should be emphasized, is that the damage index method is the only method tested that has a specific criterion for determining whether damage has occurred at a particular location. The other methods only look for the largest change in a particular parameter and it is ambiguous at times to determine whether these changes indicate damage at more than one location. However, this same criterion used with the damage index method could be easily adapted to the other four methods as well. The criterion used

Table 5. Summary of damage detection results applied to numerical modal data.

Damage case	Damage index method	Mode shape curvature method	Change in flexibility method	Change in uniform load surface curvature method	Change in stiffness method
A-1: 3.5′ web cut to topside of bottom flange positioned at the girder mid-span	••	○	○	○	○
A-2: 3.5′ web plus half of bottom flange cut positioned at the girder mid-span	••	○	○	○	○
A-3: 3.5′ web plus full bottom flange cut positioned at the girder mid-span	•	•	○	•	○
A-4: 3.5′ web plus full bottom flange cut positioned 40′ from the interior support	•	•	•	•	•
A-5: 3.5′ web plus full bottom flange cut positioned 20′ from the interior support	•	•	•	•	•
A-6: 3.5′ web plus full bottom flange cuts positioned 40′ from the interior support and 20′ from the girder mid-span	• one damage location was not identified	•	•	•	•
A-7: 3.5′ web cut to topside of bottom flange positioned 40′ from the interior support	○	•	○	○	○
A-8: 3.5′ web cut to topside of bottom flange positioned 20′ from the interior support	••	•	○	•	○
A-9: two undamaged data sets		false-positive indication of damage	false-positive indication of damage	false-positive indication of damage	false-positive indication of damage

• damage located; •• damage narrowed down to two locations; ••• narrowed down to three locations; ○ damage not located.

by the damage index method for determining whether a change in the damage index corresponds to actual damage is to look for statistical outliers in the population of all damage indices. It is the authors' opinion, though again not rigorously verified analytically, that this method will have difficulties if numerous damage locations are present (implying that the outliers will be closer to the mean) as was indicated by damage case A-6.

The authors acknowledge that recently reported improvements to the damage identification methods used in this study may offer enhanced capabilities to detect damage from changes in measured modal properties. As an example, Doebling (1995) investigated the problem of assembling flexibility matrices from measured modal data. Methods for calculating residual flexibilities (the contribution of the unmeasured modes to the flexibility matrix) were developed and shown effective in improving the accuracy of the flexibility matrices. A more refined application of the change in stiffness method to the I-40 bridge can be found in James *et al* (1995). In this investigation, an attempt was made to derive mass and stiffness matrices, which better resemble the properties of the structure, by assuming a certain connectivity between the sensors. Under this assumption, terms of the mass and stiffness matrices not reflective of the assumed sensor connectivity are forced to zero. The matrices are further modified by separating the portion reflective of the assumed connectivity from the portion not reflective of the assumed connectivity. By considering the mass and stiffness matrices associated with the assumed model of the structure, the performance of the change in stiffness method was improved.

It is the authors' hope that these analytical data sets along with the experimental data sets discussed in the accompanying paper can be used as a set of benchmark problems for comparison of future damage detection methods. To this end, these data sets and the numerical models have been provided to several universities and national laboratories for additional study. Future numerical studies should investigate the influence of the excitation location on the ability to identify damage and investigate the ability to identify damage when damage is not located near a sensor. A numerical and corresponding experimental study similar to the one reported herein, but performed on simple structural elements such as beams and plates, is currently being performed with the intent to provide a more basic understanding of the differences in the various damage identification methods. Finally, as with the accompanying experimental study, the authors acknowledge that the results reported in this study are valid

only for the structure analysed and are based on a limited number of numerically simulated experiments. A large data base of various structure types and damage scenarios must be investigated before general statements regarding the relative merits of the various damage identification methods can be stated absolutely.

Acknowledgments

Funding for this research was provided to New Mexico State University (NMSU) by the Federal Highway Administration. NMSU, in turn, contacted Los Alamos National Laboratory to perform the analyses reported herein. Additional funding was provided by Los Alamos National Laboratory's Laboratory Directed Research and Development program. Work was performed under the auspices of the US Department of Energy.

References

Clough R W and Penzien J 1993 *Dynamics of Structures* 2nd edn (New York: McGraw-Hill)

Doebling S W 1995 Measurement of structural flexibility matrices for experiments with incomplete reciprocity *Doctoral Dissertation* Department of Aerospace Engineering, University of Colorado

Doebling S W *et al* 1996 Damage identification in structures and mechanical systems based on changes in their vibration characteristics: a detailed literature review *Los Alamos National Laboratory Report* LA-13070-MS

Ewins D J 1985 *Modal Testing: Theory and Practice* (New York: Wiley)

Farrar C R, Baker W E, Bell T M, Cone E M, Darling T W, Duffey T A, Eklund A and Migliori A 1994 Dynamic characterization and damage detection in the I-40 bridge over the Rio Grande *Los Alamos National Laboratory Report* LA-12767-MS

Farrar C R, Duffey T A, Goldman P A, Jauregui D V and Vigil J S 1996 Finite element analysis of the I-40 bridge over the Rio Grande *Los Alamos National Laboratory Report* LA-12797-MS

Farrar C R and Jauregui D 1996 Damage detection algorithms applied to experimental and numerical modal data from the I-40 bridge *Los Alamos National Laboratory Report* LA-13074-MS

——1998 Comparative study of damage identification algorithms applied to a bridge: I. Experiment *Smart Mater. Struct.* at press

Hibbitt, Karlsson and Sorensen 1994 *ABAQUS Theory Manual* version 5.4 (Providence, RI: Hibbitt, Karlsson and Sorensen)

James G, Mayes R, Carne T, Simmermacher T and Goodding J 1995 Health monitoring of operational structures—initial results *Proc. 36th AIAA/ASME/ASCE/AHS/ASC Structures, Structural Dynamics, and Materials Conf.*

MathWorks 1992a *MATLAB Reference Guide* (Natick, MA: MathWorks)

——1992b *MATLAB User's Guide* (Natick, MA: MathWorks)

——1992c *Signal Processing Toolbox* (Natick, MA: MathWorks)

Pandey A K and Biswas M 1994 Damage detection from changes in flexibility *J. Sound Vib.* **169** 3–17

Pandey A K, Biswas M and Samman M M 1991 Damage detection from changes in curvature mode shapes *J. Sound Vib.* **145** 321–32

Stubbs N and Kim J-T 1994 Field verification of a nondestructive damage localization and severity estimation algorithm *Texas A&M University Report prepared for New Mexico State University*

Zhang Z and Aktan A E 1995 The damage indices for the constructed facilities *Proc. 13th Int. Modal Analysis Conf.* vol 2, pp 1520–9

Zimmerman D C and Kaouk M 1994 Structural damage detection using a minimum rank update theory *J. Vib. Acoust.* **116** 222–31